IMMUNOLOGY

T Cell Activation Results in Conformational Changes in the Src Family Kinase Lck to Induce Its Activation

Anja Stirnweiss,[1]* Roland Hartig,[1] Steffi Gieseler,[1]† Jonathan A. Lindquist,[1] Peter Reichardt,[1] Lars Philipsen,[1] Luca Simeoni,[1] Mateusz Poltorak,[1] Camilla Merten,[1] Werner Zuschratter,[2] Yury Prokazov,[2] Wolfgang Paster,[3]‡ Hannes Stockinger,[3] Thomas Harder,[1] Matthias Gunzer,[1]§ Burkhart Schraven[1,4]‖

The lymphocyte-specific Src family protein tyrosine kinase p56^{Lck} (Lck) is essential for T cell development and activation and, hence, for adaptive immune responses. The mechanism by which Lck activity is directed toward specific substrates in response to T cell receptor (TCR) activation remains elusive. We used fluorescence lifetime imaging microscopy to assess the activation-dependent spatiotemporal changes in the conformation of Lck in live human T cells. Kinetic analysis of the fluorescence lifetime of Lck biosensors enabled the direct visualization of the dynamic local opening of 20% of the total amount of Lck proteins after activation of T cells with antibody against CD3 or by superantigen-loaded antigen-presenting cells. Parallel biochemical analysis of TCR complexes revealed that the conformational changes in Lck correlated with the induction of Lck enzymatic activity. These data show the dynamic, local activation through conformational change of Lck at sites of TCR engagement.

INTRODUCTION

Src family tyrosine kinases (SFKs) trigger numerous cellular processes, including proliferation, differentiation, adhesion, and migration. The SFK family member p56^{Lck} (referred to as Lck) critically induces T cell responses after activation of cell surface receptors. Lck-deficient peripheral T cells cannot be activated through the T cell receptor (TCR). Consequently, T cell development is severely impaired in the absence of Lck (*1*). Phosphorylation of immunoreceptor tyrosine-based activation motifs (ITAMs) within the TCR-associated CD3 and ζ chains by Lck is one of the earliest detectable events after TCR stimulation, and it initiates multiple signaling cascades that culminate in T cell activation and proliferation (*2*); however, despite years of research, the molecular events preceding ITAM phosphorylation are poorly understood. Changes in the accessibility of ITAM-containing substrates and in the catalytic activity of Lck have been proposed to contribute to the initiation of signaling after TCR stimulation.

The activity of SFKs is tightly controlled by structural dynamics that are highly conserved between members and across species (*3*). Accordingly, the activity of Lck is controlled by conformational changes that arise from phosphorylation and dephosphorylation of two critical tyrosine residues, Tyr^{394} and Tyr^{505} (*4*). When phosphorylated by the C-terminal Src kinase (Csk), the C-terminal tyrosine residue Tyr^{505} inhibits Lck activity (*5*, *6*). Phosphorylation of the inhibitory tyrosine induces an intramolecular association with the Src homology 2 (SH2) domain, causing the kinase to adopt a closed, "inactive" conformation (*3*, *7*), which is stabilized by an additional interaction between the SH3 domain and a polyproline helix within the linker region (*7*, *8*). The plasma membrane–localized tyrosine phosphatase CD45 counteracts Csk by dephosphorylating Tyr^{505}, thereby generating a pool of Lck in an open, "primed" conformation (*9*, *10*). Ligand binding to the SH2 and SH3 domains of Lck may additionally contribute to its activation (*11*–*13*). Activation of Lck is thought to depend on the autophosphorylation of Tyr^{394} within the activation loop of the kinase domain (*14*). Only Lck molecules phosphorylated on Tyr^{394} show enhanced enzymatic activity and facilitate substrate phosphorylation (*15*, *16*).

Nika *et al*. demonstrated that in resting T lymphocytes, as well as in nonstimulated Jurkat cells (a human CD4$^+$ leukemic T cell line), a substantial amount of Lck exists in a constitutively active (Tyr^{394}-phosphorylated) form (*17*). The authors described four pools of Lck in resting T cells: (i) closed, inactive Lck (Tyr^{505}-phosphorylated); (ii) primed (nonphosphorylated); (iii) active Lck (Tyr^{394}-phosphorylated); and (iv) active, doubly phosphorylated (DPho) Lck (phosphorylated on both Tyr^{394} and Tyr^{505}). In Jurkat cells, each pool constitutes about 25% of the total amount of Lck, whereas in resting human T cells, about 50% of the total Lck protein is primed (*17*). Nika *et al*. did not observe changes in the enzymatic activity of Lck upon stimulation of the TCR. The authors concluded that the Lck-dependent tyrosine phosphorylation of ITAMs does not result from TCR-mediated de novo activation of Lck, but rather from other mechanisms, such as the relocalization of active Lck within the cell or from ligand-mediated conformational changes within the TCR (*18*, *19*).

[1]Institute of Molecular and Clinical Immunology, Otto von Guericke University, Leipziger Strasse 44, 39120 Magdeburg, Germany. [2]Leibniz Institute for Neurobiology, Brenneckestrasse 6, 39118 Magdeburg, Germany. [3]Molecular Immunology Unit, Institute for Hygiene and Applied Immunology, Center for Physiology, Pathophysiology, and Immunology, Medical University of Vienna, Lazarettgasse 19, A-1090 Vienna, Austria. [4]Department of Immune Control, Helmholtz Centre for Infection Research, 38124 Braunschweig, Germany.
*Present address: Division of Children's Leukaemia and Cancer Research, Telethon Institute for Child Health Research, 100 Roberts Road, Subiaco, WA 6008, Australia.
†Present address: Children's Hospital, Otto von Guericke University, Leipziger Strasse 44, 39120 Magdeburg, Germany.
‡Present address: T Cell Signalling Laboratory, Sir William Dunn School of Pathology, University of Oxford, South Parks Road, Oxford OX1 3RE, UK.
§Present address: Institute for Experimental Immunology and Imaging, University Hospital, University of Duisburg/Essen, Universitätsstraße 2, 45117 Essen, Germany.
‖To whom correspondence should be addressed. E-mail: Burkhart.Schraven@med.ovgu.de

To assess the potential role of the conformational dynamics of Lck in T cell activation, Paster *et al.* constructed a biosensor consisting of the complete Lck backbone flanked by enhanced cyan fluorescent protein (ECFP) and enhanced yellow fluorescent protein (EYFP) (*20*), which act respectively as donor and acceptor fluorophores for Förster resonance energy transfer (FRET). When the Lck biosensor molecule is in the active, open conformation, FRET is low, whereas a closed enzyme (inactive, Tyr^{505}-phosphorylated) produces a strong FRET signal. With this Lck biosensor, the authors measured FRET with intensity-based detection techniques and observed no substantial changes in the FRET efficiency of the biosensor upon TCR-mediated activation of Jurkat cells (*20*, *21*).

We investigated the conformational dynamics of Lck in response to TCR activation with an alternative technique to monitor FRET. FRET affects the mean lifetime for which the donor fluorophore molecules remain in the excited state before they relax back to the ground state and release a photon. Through the use of fluorescence lifetime imaging microscopy (FLIM) (*22*, *23*), we recorded, at microscopic resolution, donor fluorescence decay kinetics, which enabled the measurement of FRET independently of fluorophore concentrations. We used a new time domain FLIM strategy to follow the conformational dynamics of the Lck biosensor of Paster *et al.* The greatly improved signal-to-noise ratio obtained with our strategy enabled us to directly measure and visualize the conformational opening of Lck upon TCR activation in live T cells. Moreover, in vitro kinase assays revealed that the opening of Lck correlated with the enhanced enzymatic activity of the kinase.

RESULTS

A fluorescence-based Lck biosensor rescues signaling in Lck-deficient Jurkat cells

To identify changes in the conformational states of Lck in live cells, we used a unimolecular biosensor consisting of the complete Lck backbone flanked by ECFP and EYFP, which acted as donor and acceptor fluorophores, respectively (CLckY-1; Fig. 1A) (*20*). To assess the function of the biosensor, we expressed it in the Lck-deficient Jurkat cell line JCam1.6, which is unresponsive to TCR-mediated signals (*24*). Expression of CLckY-1 in JCam1.6 cells reconstituted global tyrosine phosphorylation (Fig. 1B) and Ca^{2+} flux in response to soluble stimulation with a monoclonal antibody against CD3 (αCD3) similar to that in Jurkat cells that express wild-type Lck (Fig. 1, C and D).

Spectral measurements reveal the FRET behavior of the CLckY-1 biosensor

To distinguish the true FRET events of the biosensor from other excited state reactions, we recorded intensity spectra with a time-resolved,

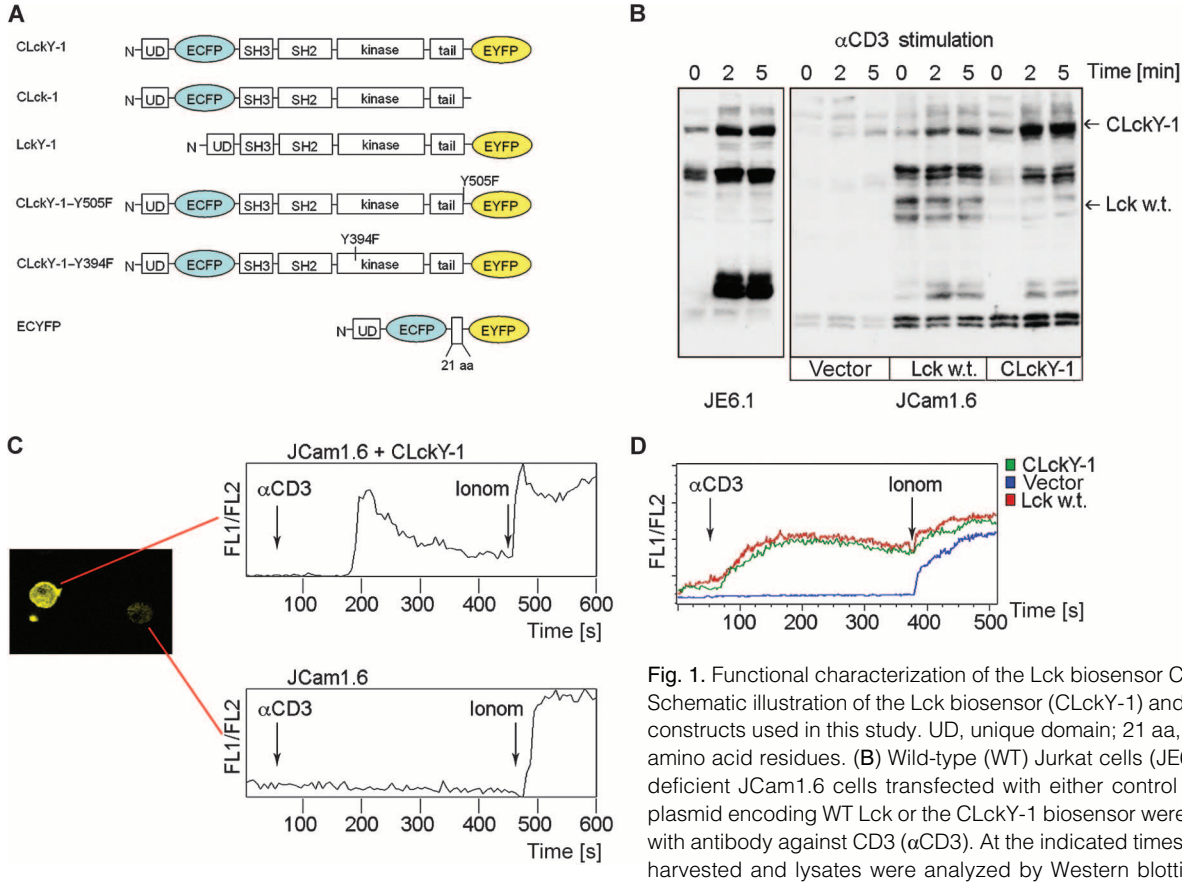

Fig. 1. Functional characterization of the Lck biosensor CLckY-1. (**A**) Schematic illustration of the Lck biosensor (CLckY-1) and the control constructs used in this study. UD, unique domain; 21 aa, linker of 21 amino acid residues. (**B**) Wild-type (WT) Jurkat cells (JE6.1) or Lck-deficient JCam1.6 cells transfected with either control plasmid or plasmid encoding WT Lck or the CLckY-1 biosensor were stimulated with antibody against CD3 (αCD3). At the indicated times, cells were harvested and lysates were analyzed by Western blotting for total tyrosine phosphorylation with the antibody 4G10. A typical result from one of three independent experiments is shown. (**C** and **D**) JCam1.6 cells transfected as described in (B) were loaded with the Ca^{2+}-sensitive dye Indo-1 AM. Ca^{2+} mobilization of cells after treatment with αCD3 or ionomycin (Ionom) was measured either (C) by confocal microscopic analysis of individual cells, which showed that only transfected cells responded to antibody stimulation, or (D) by bulk analysis by flow cytometry measured at a flow rate of 300 cells s^{-1}. Representative results out of three (for confocal analysis) or five (for flow cytometric analysis) independent experiments are shown.

microspectroscopic delay line (DL) detector. To generate a FRET-positive control, we transfected cells with a plasmid encoding a plasma membrane–anchored fusion protein in which the donor and acceptor fluorophores were separated by 21 amino acid residues (ECYFP; Fig. 1A). Because of the close proximity of the fluorophores, ECYFP reports on the maximal possible FRET signal. We also used a variant of CLckY-1 in which Tyr^{394} was mutated to phenylalanine (CLckY-1–Y394F; Fig. 1A). This Y394F mutation induces formation of the closed conformation of Lck (*20*); hence, the FRET of CLckY-1–Y394F reports on a fraction of the Lck biosensor that is in the constitutively closed conformation, which is expected to be greater than that of CLckY-1. As a FRET-negative control, we generated CLckY-1–Y505F, in which the C-terminal negative regulatory residue Tyr^{505} was mutated to phenylalanine (Fig. 1A). This mutation prevents the intramolecular interaction between the C terminus and the SH2 domain of Lck, thus generating a constitutively open conformation that exhibits a low FRET efficiency (*20*).

At an excitation wavelength of 420 nm, which excites the donor ECFP only, the intensity spectra of all constructs showed a first peak at 475 nm (Fig. 2A). This peak represents the characteristic emission spectrum of the donor (ECFP). A prominent second peak at 525 nm indicates the FRET-induced fluorescence of the acceptor (EYFP) and marks the FRET signal of the positive control (ECYFP). The peak at 525 nm was also observed in the biosensor molecules (Fig. 2A). As expected, the peak intensity was highest in the spectrum of the Lck Y394F biosensor, lower in the wild-type Lck biosensor (CLckY-1), and undetectable in cells with the FRET-negative control (CLckY-1–Y505F), consistent with the constitutively open conformation of this mutant Lck.

To differentiate between inter- and intramolecular FRET, we compared the fluorescence spectra of JCam1.6 cells expressing the CLckY-1 biosensor with those of cells expressing a version that contained only ECFP (donor-tagged Lck, CLck-1; Fig. 1A) and cells that coexpressed donor-only (CLck-1) and acceptor-only (LckY-1) tagged biosensors (Fig. 1A). A FRET-specific peak at 525 nm was not detectable in cells expressing CLck-1 alone or in those coexpressing CLck-1 and LckY-1 (Fig. 2B). Hence, the FRET signals measured in cells expressing Lck biosensor variants were caused by intramolecular energy transfer and correlated with the conformational states of the Lck biosensors.

FLIM discriminates between the individual kinetic components of ECFP fluorescence

For unknown molecular reasons, not all ECFP molecules mediate FRET (*25*). Thus, a subfraction of the ECFP molecules that undergo a change in FRET may escape detection against a background of fluorescence signal from molecules that do not undergo FRET. To tackle these inherent problems of the low signal-to-noise ratio in FRET measurements,

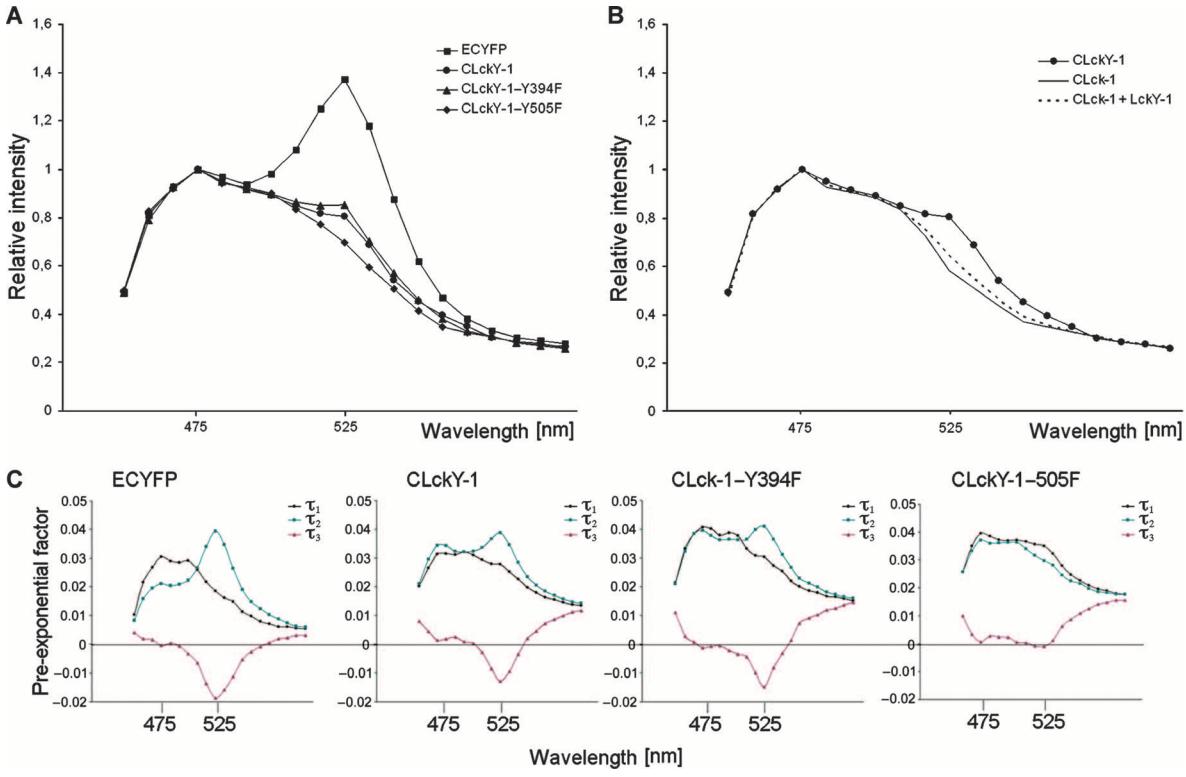

Fig. 2. Microspectroscopic characterization of CLckY-1 and different control constructs. (**A** and **B**) Spectral emissions along a wavelength range of 460 to 650 nm were resolved and collected by the DL detector after excitation at 420 nm. Represented are the relative fluorescence intensities against the emission wavelength of five independent measurements for JCam1.6 cells transfected with the appropriate plasmids encoding (A) ECYFP, CLckY-1, CLckY-1–Y394F, or CLckY-1–Y505F or (B) CLckY-1, CLck-1, or CLck-1 and LckY-1. (**C**) DAS spectra of the measurements shown in (A) and (B) of ECFP subpopulations that were identified by a three-exponential fit of the experimental data with individual characteristic lifetimes of τ_1 (3.2 ns), τ_2 (1.4 ns), and τ_3 (0.8 ns), respectively. Diagrammed are the changes in the pre-exponential factors of the three lifetimes as a function of the wavelengths for ECYFP, the Lck-biosensor CLckY-1, CLckY-1–Y394, and CLckY-1–Y505F. Negative pre-exponential factors result from FRET between the donor and acceptor.

we made use of detailed characterizations of the decay kinetics of ECFP fluorescence. Our work and that of others showed that in an ECFP-EYFP FRET pair, the mean decay of ECFP fluorescence, described by the mean lifetime τ_{mean}, can be fitted with three exponential decay components. These kinetic components are defined by three individual decay lifetimes: τ_1, τ_2, and τ_3, which characterize individual subpopulations of fluorophore pairs that can be individually selected for FRET measurements (*26–31*). We applied a Levenberg-Marquardt nonlinear, least-squares algorithm to dissect the decay kinetics of ECFP fluorescence in the Lck biosensor into individual lifetimes. A three-exponential fit resulted in a precise ($\chi^2 < 1.3$) description of the experimental data and revealed three individual τ values of ECFP within the biosensor of 3.2 ns (τ_1), 1.4 ns (τ_2), and 0.8 ns (τ_3), respectively. The fractional distributions of the individual lifetimes were calculated as 40% (τ_1), 35% (τ_2), and 25% (τ_3).

Analysis of decay-associated spectra identifies the ECFP subpopulation of the Lck biosensor involved in FRET

Plotting the pre-exponential factors of the individual lifetimes against the emission wavelength yielded the decay-associated spectra (DAS) (Fig. 2C), which were used to identify those ECFP molecules engaged in FRET. When the component undergoes FRET, the pre-exponential factor of an individual lifetime acquires a more negative value relative to the baseline at the emission wavelength of the acceptor. At the acceptor emission maximum of 525 nm, only τ_3 acquired negative values in Jurkat cells expressing ECYFP, CLckY-1, or CLckY-1–Y394F (Fig. 2C). Comparing the FRET signals of these constructs led to the following arrangement of FRET signals: ECYFP > CLckY-1–Y394F > CLckY-1. No negative value for τ_3 was found in cells expressing the constitutively open CLckY-1–Y505F, which indicated that among the three components contributing to the mean fluorescence decay of ECFP, only τ_3 was affected by FRET. In addition, τ_3 contributed to 25% of

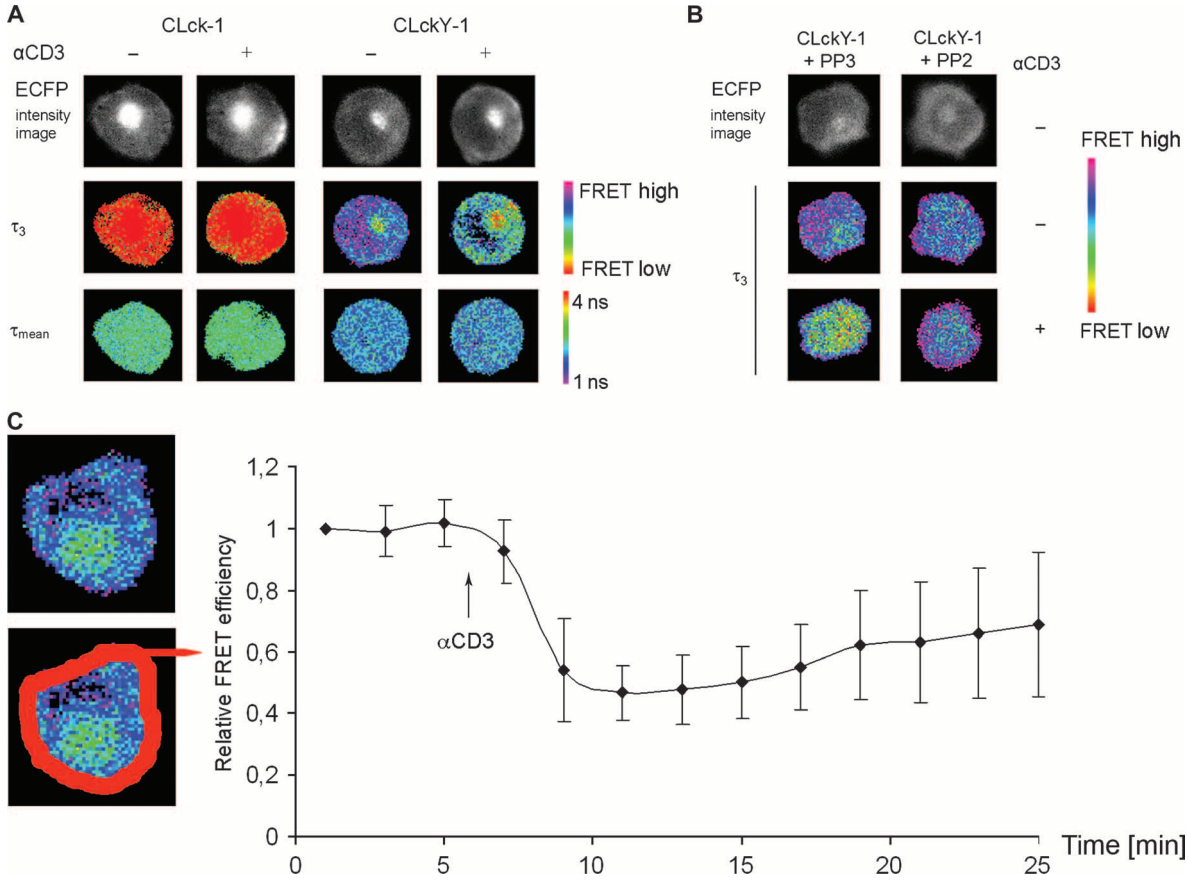

Fig. 3. Conformational changes in the Lck biosensor in response to stimulation of cells with anti-CD3 antibody. (**A** to **C**) Live JCam1.6 cells that had been transfected with plasmid encoding the biosensor (CLckY-1) or with a control plasmid lacking the FRET acceptor EYFP (CLck-1) were analyzed with the QA detector. After excitation at 420 nm, the spectral emissions of the FRET donor ECFP were detected at 465 to 485 nm. Data from at least three independent experiments were analyzed, and representative results are shown in (A) and (B). (A and B) ECFP intensity images captured by the QA detector are represented in the upper panels. (A to C) Pseudocolored images for the pre-exponential factors of τ_3 and τ_{mean} revealed the location of FRET events within the cells. Purple to blue pixels correspond to closed Lck molecules (high FRET), whereas yellow to red pixels indicate molecules with low FRET because of an open conformation of the Lck biosensor. (A) JCam1.6 cells transfected with plasmids encoding CLckY-1 or CLck-1 before and 7 min after stimulation with αCD3. (B) JCam1.6 cells transfected with plasmid encoding CLckY-1 were pretreated for 30 min with 10 μM PP2 or 10 μM PP3. Nonstimulated cells and cells stimulated with αCD3 for 7 min are depicted. (C) Time-resolved analysis of changes in the pre-exponential factor of τ_3 at the plasma membrane of JCam1.6 cells transfected with plasmid encoding CLckY-1 (n = 10 cells, from n = 3 independent experiments; data are means ± SD). The measured area in the lower micrograph is highlighted in red.

the total mean lifetime and therefore may remain undetected when conventional methods of FRET detection, such as intensity-based measurements or mean lifetime FLIM measurements, are applied.

The biosensor reports on the conformational dynamics of Lck at sites of TCR activation in Jurkat cells

Next, we investigated whether Lck underwent conformational change upon T cell activation. We expressed the biosensor or the donor-only tagged variants in JCam1.6 cells and measured the fluorescence lifetimes with the position-sensitive photomultiplier (QA detector) (*32*) to resolve the spatial distribution, as well as the three individual lifetimes of the biosensor (fig. S1). Both CLck-1 and CLckY-1 localized to two major areas, the plasma membrane and a cytoplasmic compartment that partially overlap with early endosomes but not with the endoplasmic reticulum or the Golgi apparatus (Fig. 3A and figs. S2 and S3). Similar subcellular distributions of Lck have been reported previously (*33*–*35*).

FLIM analysis focusing on τ_3 within the CLckY-1 biosensor detected a constitutively open Lck population (low FRET) at the plasma membrane of Jurkat cells and in the cytoplasmic compartment (Fig. 3A, right panels, middle row). Upon treatment with PP2, an inhibitor of SFKs, but not with the inactive analog PP3, these open CLckY-1 molecules became undetectable, and the biosensor assumed the closed conformation (Fig. 3B, middle panels). These data indicate that the open Lck molecules in unstimulated Jurkat cells were constitutively active, which confirmed previous data (*17*).

We then investigated whether Lck underwent conformational changes upon T cell activation. Stimulation with αCD3 induced a detectable decrease in the pre-exponential factors of τ_3 at the plasma membrane and in the cytoplasmic compartment of cells with the CLckY-1 biosensor (Fig. 3A, middle right panels), but not in cells with the ECFP-only variant CLck-1 (Fig. 3A, middle left panels). Opening of the biosensor at the plasma membrane was observed to last for at least 20 min (Figs. 3C and 4A). Again, the decrease in FRET upon T cell activation was completely lost when the cells were pretreated with PP2 (Fig. 3B, lower panels). Together, the behavior of τ_3 in αCD3-stimulated Jurkat cells showed that T cell activation induced an opening of the biosensor. This finding suggested that Lck became activated by a

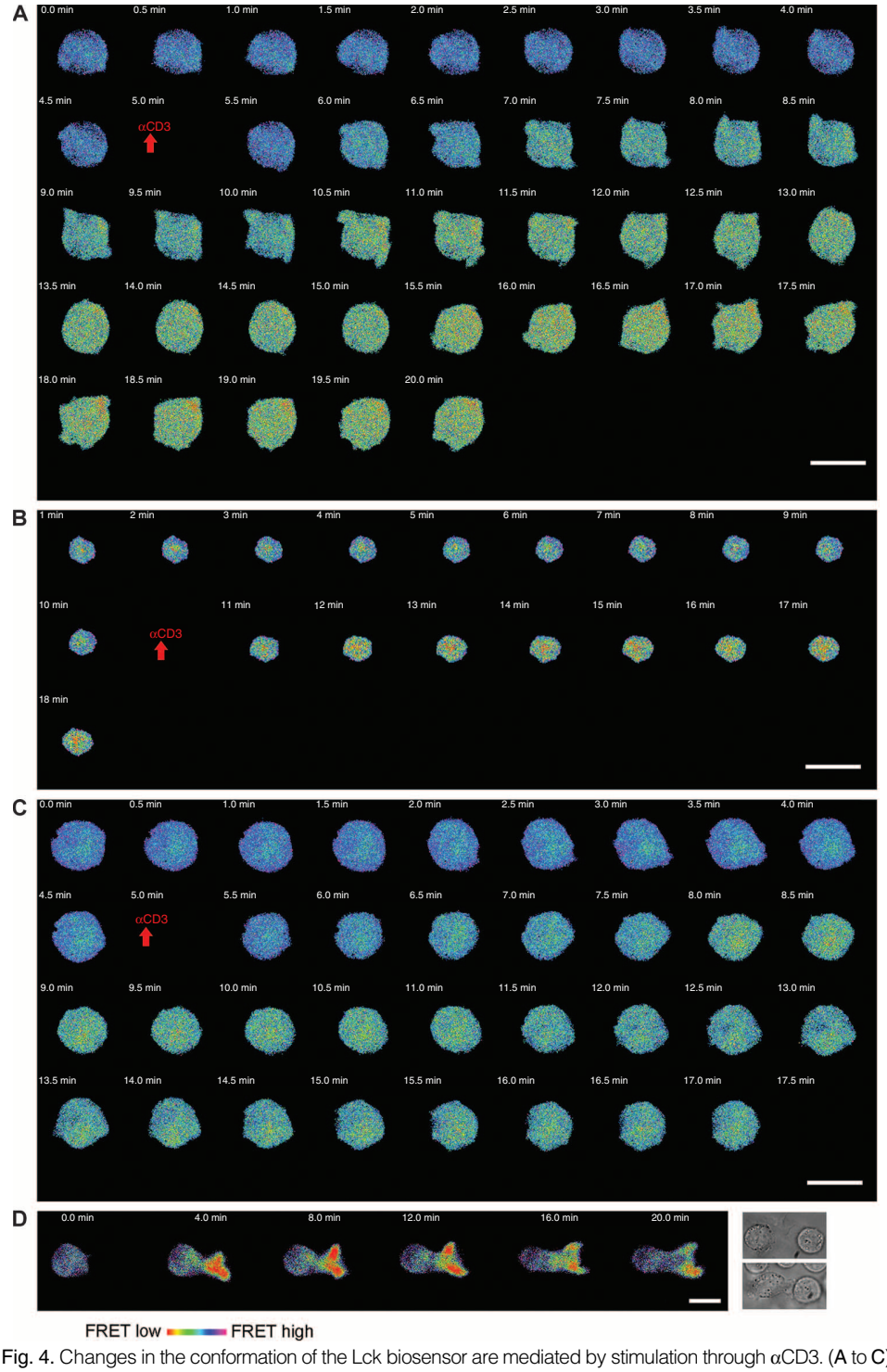

Fig. 4. Changes in the conformation of the Lck biosensor are mediated by stimulation through αCD3. (**A** to **C**) Pseudocolored FLIM images measured with the QA detector represent the pre-exponential factors of τ_3 in (A) JCam1.6 cells, (B) human T cells, and (C) Zap70-deficient P116 cells expressing CLckY-1. (**D**) In Jurkat cells stimulated with SEE-loaded Raji B cells (APCs), the Lck biosensor adopts an open conformation at the site of contact between the Jurkat cell and the APC. The transmitted light images show CLckY-1–expressing Jcam1.6 cells before and after contact with SEE-loaded Raji B cells. Representative images of cells are shown from 30 (A), 10 (B), 12 (C), and 10 (D) measurements from three independent experiments each. Scale bars, 10 μm.

conformational change immediately after stimulation of cells with αCD3. The constitutively open Lck molecules in unstimulated cells and the activation-induced decrease in FRET could only be observed by combining FLIM measurements with an analysis of the pre-exponential factors of τ_3, the characteristic lifetime of the subpopulation of the donor molecules involved in the FRET process. We did not detect alterations in the mean lifetime of the FRET signal in stimulated cells that had the CLckY-1 biosensor (Fig. 3A, lower panels). This observation corroborates the data of Paster *et al*. (*20*).

Table 1. Changes in T_{mean} and the pre-exponential factors of τ_3 of a JCam1.6 cell expressing the biosensor after TCR stimulation. The time range of 0 to 2 min was used as the reference point. n.d., not detectable.

Time points (min)	τ_{mean} (ns)	Change of τ_{mean} (%)	Change of fractional distribution of τ_3 (%)
0–2	2.82	—	—
7–9	2.82	n.d.	16
13–15	2.83	n.d.	20
18–20	2.84	n.d.	35

We then analyzed the tracks of TCR-mediated conformational changes in the Lck biosensor as visualized by FLIM over time after TCR stimulation (Fig. 4). Activation-induced opening of the Lck biosensor was observed in JCam1.6 cells (Fig. 4A) and in primary human T lymphocytes (Fig. 4B). The opening of the biosensor was already detectable just 1 min after application of the αCD3 antibody. Similarly, rapid opening of the biosensor was also observed in the ζ chain–associated protein kinase of 70 kD (Zap70)–deficient Jurkat variant P116 cells, which rules out the possibility that TCR-mediated opening of the biosensor in transfected JCam1.6 and primary T cells was a result of the binding of the SH2 domain of Lck to phosphorylated Zap70 (Fig. 4C).

To determine the relative fraction of the open biosensor molecules in unstimulated and activated T cells, we split the data stream into 2-min time windows. Photons collected during the first 2 min were defined as the baseline value. With this approach, we found that 16% of the biosensor molecules involved in FRET showed an open conformation before stimulation. After 5 min, the cell was stimulated with αCD3 antibody. Continuously recorded FLIM data were analyzed at the time points 0 to 2, 7 to 9, 13 to 15, and 18 to 20 min (Table 1), and the fractional intensities were calculated. This calculation showed that TCR stimulation induced a continuous decrease in the FRET signal (equivalent to opening of the Lck molecule) of an additional 20% of the biosensor molecules undergoing FRET at the plasma membrane (Table 1).

To visualize the conformational changes in the biosensor under more physiological conditions, we monitored the spatiotemporal changes in Lck conformation in a T cell activation model system in which the TCR was triggered by contact with antigen-presenting cells (APCs). We incubated superantigen (SEE)–loaded Raji B cells with Jurkat cells expressing the biosensor. Changes in FRET signals reported the rapid accumulation of the open, activated conformation of the Lck biosensor at the contact zone between both cell types (Fig. 4D). No changes in biosensor FRET occurred in conjugates of T cells with nonpulsed APCs (fig. S4), indicating that opening of the biosensor required engagement of the TCR.

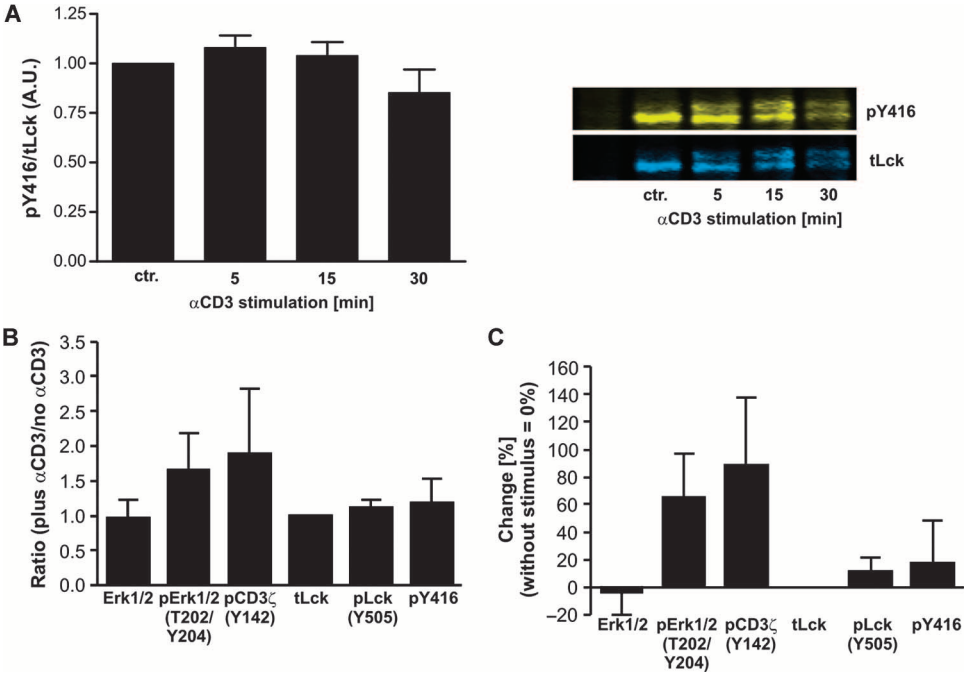

Fig. 5. Global analysis of Lck phosphorylation after T cell activation. (**A**) Lysates of unstimulated, control Jurkat cells (ctr.) and cells stimulated for the indicated times with αCD3-coated microbeads were subjected to immunoprecipitations. The Lck immunoprecipitates were analyzed in a dual fluorescence Western blot (right panel) with αLck (blue) and antibodies against Src family kinases containing $pTyr^{416}$, which label the corresponding $pTyr^{394}$ of Lck (yellow). The ratios of signals from tyrosine-phosphorylated Lck and total Lck protein were calculated from four independent experiments and are shown in the bar graph on the left as means ± SD. (**B** and **C**) MELK analysis: quantification of changes in signal intensities of the displayed signaling molecules after stimulation of Jurkat JE6.1 cells with αCD3 for 5 min. (B) Ratio of the signals of the indicated proteins between αCD3-stimulated and unstimulated Jurkat cells (mean ± SD). (C) Relative changes in the fluorescence signal ratios between stimulated and nonstimulated cells (mean ± 95% confidence interval). Data are combined from six independent experiments in which a total of 448 cells were analyzed.

The enzymatic activity of Lck is enhanced upon T cell activation

A fraction of Lck molecules underwent conformational changes upon T cell activation, in apparent disagreement with Nika *et al*., who proposed that activation of T cells is not accompanied by increased pools of activated Lck. Consistent with this proposal, we observed that Lck in total cell lysates obtained from αCD3-stimulated primary human T cells showed no substantial increase in the Lck-activating Tyr^{394} phosphorylation (Fig. 5A). We obtained similar results when we examined the phosphorylation status of Lck by automated multidimensional fluorescence microscopy [multi-epitope ligand

cartography (MELK)], which enables simultaneous imaging of several signaling molecules within the same cell (Fig. 5, B and C). However, when we subjected Lck immunoprecipitated from resting or αCD3-stimulated human T lymphocytes or Jurkat cells to a classical in vitro kinase assay with radiolabeled adenosine 5′-triphosphate (ATP), we observed a 20% increase in Lck activity in four independent experiments with each cell type after 30 and 120 s of stimulation (Fig. 6). The increase in Lck phosphorylation was not a consequence of coimmunoprecipitation of Lck with Csk (fig. S5) and correlated well with our FLIM data, which showed that 20% of the biosensor molecules locally adopt an open active conformation at sites of TCR activation.

DISCUSSION

One of the first biochemical events after stimulation of the TCR is the phosphorylation of ITAMs within the TCR by the SFK Lck; however, very little is known about the regulation of Lck activity after T cell activation. With a FRET-based Lck biosensor and a new FLIM-based strategy, we assessed the intracellular conformation of Lck in unstimulated and TCR-stimulated Jurkat cells and primary human T lymphocytes. In unstimulated Jurkat cells, a fraction of the biosensor (and hence of Lck) was found in a constitutively open conformation. These open Lck molecules rapidly assumed a closed conformation when cells were treated with the SFK-specific inhibitor PP2. This suggests that the open fraction of Lck represents constitutively active Lck molecules, corroborating the data of Nika *et al*., who identified constitutively active forms of Lck in resting T cells (*17*). Mechanistically, PP2 induced a reduction in the extent of Tyr^{394} phosphorylation, which most likely was mediated by the transmembrane phosphatase CD45. Our FLIM measurements provide a direct demonstration of conformational changes in an SFK in live cells as a result of a change in its phosphorylation status. TCR activation induced the rapid opening of the Lck biosensor in T cells, including the Zap70-deficient P116 Jurkat variant cell line. This suggests that the binding of Lck to tyrosine-phosphorylated Zap70 through its SH2 domain (*36*) is not required for the conformational opening of Lck at sites of TCR activation.

Our FLIM and biochemical measurements conflict with reports that suggest that Lck changes neither its conformation nor its enzymatic activity upon T cell activation. Paster *et al.* did not detect changes in FRET efficiency, as a measure of conformational changes, with an Lck biosensor similar to the one that we used here (*20*). We attribute this discrepancy to the FRET detection technique that was used by Paster *et al*., namely, a fluorescence intensity–based method that monitors the integral of the mean fluorescence. Indeed, if considering the mean lifetimes of donor fluorescence, our results fit with those of Paster *et al*. This finding shows an advantage of our method, which focuses on the analysis of the subpopulation of donor molecules that is engaged in FRET. Antibody-based approaches led Nika *et al.* to propose that T cell activation does not increase the enzymatic activity of Lck (*17*). Similarly, we did not detect substantial alterations in Lck activity when we assessed its phosphorylation status in unstimulated and stimulated T cells in experiments with phosphorylation-specific antibodies. However, when we subjected Lck immunoprecipitates from primary T cells to in vitro kinase assays, we reproducibly found an ~20% increase in the amount of autophosphorylated Lck, which correlated with our biosensor data. We attribute the apparent discrepancy between the antibody-based approaches and the in vitro kinase assays to the higher sensitivity of the radioactive assays.

We would like to emphasize that our data do not exclude the possibility that, in addition to activation of Lck, additional changes

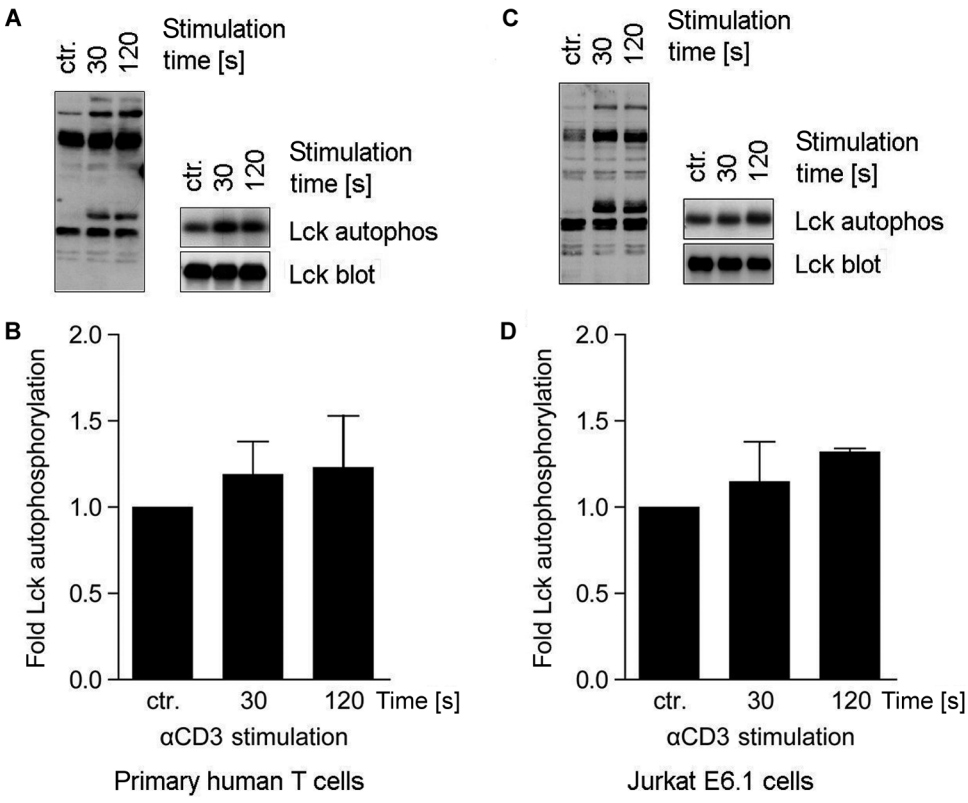

Fig. 6. Activation of Lck in primary human T cells and Jurkat E6.1 cells upon stimulation with αCD3. (A and B) Primary human T cells and (C and D) Jurkat cells were either left unstimulated as controls (ctr.) or stimulated with αCD3 for the indicated times. After lysis in buffer containing NP-40 and lauryl maltoside (LM), a fraction of the detergent lysate was subjected to SDS-PAGE and Western blotting analysis with the anti-pTyr antibody 4G10 (left panels of A and C). The remaining lysate was subjected to immunoprecipitation with antibody against Lck. Of the immunoprecipitated samples, 50% were subjected to SDS-PAGE and Western blotting analysis with anti-Lck antibody [right lower panels of (A) and (C)], whereas the remaining 50% were subjected to a classical in vitro kinase assay with radiolabeled ^{32}γ-ATP. After washing, the in vitro–labeled immunoprecipitates were subjected to SDS-PAGE, which was followed by autoradiography [right upper panels of (A) and (C)]. Data shown are a representative blot and autoradiogram from four independent experiments. (B and D) Densitometric analysis of autoradiographs of in vitro–labeled Lck immunoprecipitates obtained from unstimulated or αCD3-stimulated (B) primary human T cells or (D) Jurkat cells. The graphs show the means ± SD for the four independent experiments and indicate an increased autophosphorylation activity of Lck at 30 and 120 s after TCR activation of both cell types.

in the subcellular localization of Lck or enhanced substrate accessibility (for example, conformational changes in the TCR) contribute to ITAM phosphorylation after ligand binding. However, our data showed that a fraction of Lck adopted an open conformation and enhanced its activity after T cell activation and thus suggest that the highly conserved intramolecular regulatory mechanism of SFKs has evolved to fine-tune their activity at defined sites within T cells.

MATERIALS AND METHODS

Antibodies, cell culture, and transfection

The following antibodies were used in this study: horseradish peroxidase–conjugated mouse anti-phosphotyrosine (4G10, Millipore); mouse anti-Lck (clone 28), mouse anti-Csk, Alexa Fluor 488–conjugated mouse anti-Lck (clone 28), and Alexa Fluor 488–conjugated mouse anti-pCD3ζ (pY142, K25-407.69) (all from BD Transduction Laboratories); mouse anti-Lck (3A5, Santa Cruz Biotechnology Inc.); rabbit anti-Lck (Upstate); and rabbit anti–Src-pY416, rabbit anti-pLck (pY505), Alexa Fluor 488–conjugated mouse anti-pERK1/2 (E10), and Alexa Fluor 555–conjugated goat anti-rabbit Fab2 (all from Cell Signaling Technology). Secondary antibodies used for dual fluorescence analysis of Western blots were goat anti-rabbit IRDye 680LT and goat anti-rabbit IRDye 800CW and were obtained from LI-COR. The Jurkat cell line E6.1, the Lck-deficient variant cell line JCam1.6 (*24*, *37*), the Zap70-deficient variant Jurkat cell line P116, and the Raji B cell lymphoma cell line were obtained from the American Type Culture Collection. Cell lines were maintained in RPMI 1640 medium supplemented with 10% fetal calf serum (FCS; PAN Biotech), stable L-glutamine, penicillin (50 U/ml), and streptomycin (50 μg/ml) (Biochrom) in humidified 5% CO_2 at 37°C. Primary human T cells were isolated from healthy donors with the Pan T Cell Isolation Kit II and autoMACS (Miltenyi Biotec). The mouse anti-human CD3 monoclonal antibodies UCHT1 (eBioscience), C305 [immunoglobulin M (IgM), provided by A. Weiss, University of California San Francisco (UCSF)], and MEM92 (IgM, provided by V. Horejsi, Prague) were used to activate primary human T cells or Jurkat cells. JCam1.6 cells and P116 cells were transfected by electroporation as previously described (*38*). Briefly, 1.5×10^7 cells were transfected with 20 μg of the individual Lck-encoding plasmids or the FRET-positive control (*20*) and were analyzed 24 hours after transfection.

Fluorescence lifetime imaging microscopy

Reconstituted JCam1.6 cells (1×10^6/ml), in 1 ml of Krebs-Ringer solution [10 mM Hepes (pH 7.0), 140 mM NaCl, 4 mM KCl, 1 mM $MgCl_2$, 10 mM glucose, 1 mM $CaCl_2$], were plated on poly-L-lysine–coated glass-bottom culture disks (MatTek) for 10 min. The cells either were stimulated with soluble monoclonal antibody against human CD3ε (UCHT1, 5 μg/ml) for the indicated times or were mixed at a 1:1 ratio with Raji B cells that had been pulsed with SEE. Emission spectra (460 to 650 nm) and fluorescence lifetimes of the three pre-exponential factors of ECYFP and the different Lck constructs were determined with a microscopy system that enables time- and space-correlated single-photon counting. The imaging setup consisted of a frequency-doubled femtosecond laser (excitation wavelength, 420 nm), an inverted microscope, and two sensitive detectors: a microspectroscopic DL detector and a position-sensitive photomultiplier (QA imaging detector) (*28*, *31*, *39*, *40*). The DL detector was used to statistically analyze a very small area of the sample (with a diameter of 5 to 10 μm) and to resolve spectrally the corresponding fluorescence decays. Measurements with the QA imaging detector setup were performed to analyze the spatial distribution of the biosensors, as well as changes in their individual fluorescence lifetimes.

Analysis of FLIM data

In a multiexponential fluorescence system (for example, the ECFP-EYFP FRET pair), the intensity of the fluorescence signal decays as a sum of individual single lifetimes $I(t)$ is given by

$$I(t) = \sum_i \alpha_i \exp - t/\tau_i$$

where τ_i represents the individual decay times, and the pre-exponential factors α_i are the amplitudes of the components (indexed by i), for example, subpopulations of the fluorophore that are involved or not involved in FRET. The values of α_i and τ_i can be used to calculate the fractional distributions f_i of each of the decay times (*41*). Thus, the value of f_i represents the fractional intensities of the individual subpopulations of a mixture of fluorophores, for example, subpopulations of proteins that do or do not undergo FRET, such as ECFP.

$$f_i = (\alpha_i \tau_i)/(\sum_i \alpha_i \tau_i)$$

The values of f_i and α_i can be used to determine the mean fluorescence lifetime of each biosensor (*41*). To analyze the fluorescence decay $I(t)$, the data measured with both detectors were modeled by the convolution product of a multiexponential theoretical model with the instrument response function (IRF):

$$I(t) = \mathrm{IRF}(t) \otimes \sum_i \alpha_i \exp - t/\tau_i$$

where IRF is the measurement of the pulsed laser excitation obtained by acquiring the reflection of the laser beam. The data were analyzed by a Levenberg-Marquardt nonlinear, least-squares algorithm with the MATLAB software package, version R12.

Data acquired by the spectral (DL) detector were fitted with linked lifetimes along the wavelength band (460 to 650 nm). In this case, the intensity decay of the fluorescence signal can be described as (*41*)

$$I(\lambda, t) = \sum_i \alpha_i(\lambda) \exp - t/\tau_i$$

The wavelength-dependent pre-exponential factors $a_i(\lambda)$ of the individual lifetimes τ_i were plotted along different wavelengths, which resulted in generation of the DAS.

These spectra

$$I_i(\lambda) = \alpha_i(\lambda)\tau_i I(\lambda) \left[\sum_i \alpha_i(\lambda)\tau_i\right]^{-1}$$

represent the emission spectra of the individual components characterized by the individual lifetime τ_i (*41*). The comparison of the DAS of the individual lifetimes enables the identification of the fluorescent species (the donor and acceptor molecules) that are involved, or not, in FRET, as explained below:

Because FRET is a bimolecular process, the exited state population of the system can be described after excitation of the donor with a δ-shaped laser pulse:

$$\mathrm{d}D(t)/\mathrm{d}t = -(k_\mathrm{d} + k_\mathrm{t})D(t) \quad (1)$$

and

$$\mathrm{d}A(t)/\mathrm{d}t = D(t)k_\mathrm{t} - A(t)k_\mathrm{a} \quad (2)$$

where $D(t)$ is the concentration of the donor molecules in the exited state, $A(t)$ is the concentration of the exited acceptor molecules, k_d is the rate constant of relaxation of the donor molecules in the absence of the acceptor,

k_a is the acceptor de-excitation rate constant, and k_t is the rate constant of resonance energy transfer. The differential equations 1 and 2 describe the fluorescence decays of the donor and acceptor molecules and can be solved as follows (*42*):

$$D(t) = D_0 \exp - (k_d + k_t)t$$

$$A(t) = -D_0 k_t/(k_d + k_t - k_a)\exp - (k_d + k_t)t + D_0\ kt/(k_d + k_t - k_a)\ \exp - k_a t$$

D_0 represents the exited state population of the donor at time $t = 0$. The negative term in the function of the acceptor $A(t)$ reflects a rise component in the decay of the acceptor because of energy transfer (*42*, *43*) and results in a longer lifetime of the acceptor compared to its native lifetime. This can be detected as a negative term in the DAS in the wavelength range of the native acceptor emission wavelength (*41*). Therefore, negative terms in the DAS plot of the individual lifetimes of a multiexponential system (for example, a FRET pair consisting of fluorescent proteins) identify the subpopulation of molecules involved in the FRET process. Data collected by the QA detector were analyzed as previously described (*28*, *31*). To visualize the spatial distribution of different exited states (high or low FRET signals) of the fluorophores inside a cell, the pre-exponential factors of the lifetime τ_3, which characterizes the subpopulation of the donor molecules involved in the FRET process, were plotted as previously described (*32*). The resulting pseudocolor-coded maps show the distribution of the conformational changes of the biosensor.

Analysis of intracellular Ca^{2+} flux

JCam1.6 cells (0.3×10^6/ml) transfected with either plasmid encoding the Lck biosensor or the empty plasmid were loaded with Indo-1 AM (5 μg/ml) (Molecular Probes) for 45 min at 37°C in RPMI 1640 without phenol red (Invitrogen). After washing, cells were rested for 45 min at 37°C. Stimulation was initiated by adding 10 μl of C305 monoclonal antibody hybridoma supernatant per milliliter of cell suspension. Changes in intracellular Ca^{2+} were monitored with either a flow cytometer LSR I analyzer (BD Biosciences) or a confocal microscope Leica SP2 (Leica Microsystems Heidelberg). Cells were illuminated with the 364-nm line of an argon UV laser (for the confocal microscope) or the 325-nm laser line of a helium-cadmium laser (for the LSR flow cytometer). In both experimental settings, fluorescence emissions at 390 to 420 nm and 500 to 520 nm were detected simultaneously, and changes in the ratio of the two emission intensities were analyzed with ImageJ (confocal) or FlowJo (LSR) software, respectively. To demonstrate successful loading with the dye, we induced maximal Ca^{2+} release by adding calcium ionophore ionomycin (10 μg/ml) (Sigma-Aldrich).

Immunoprecipitations and in vitro kinase assays

To immunoprecipitate Lck (as shown in Fig. 5A), we left 5×10^6 Jurkat cells untreated or activated them with microbeads coated with anti-CD3 antibody. SuperAvidin-coated polystyrene microspheres (diameter, 10.14 μm; density, 1.6×10^7/ml; Bangs Laboratories Inc.) were incubated with the biotinylated αCD3ε monoclonal antibody UCHT1 (10 μg/ml) in phosphate-buffered saline (PBS) for 30 min at 37°C. αCD3-coated microbeads were washed twice with PBS and resuspended in RPMI 1640. Stimulation of Jurkat cells (at a cell-to-bead ratio of 2:1) was synchronized by centrifugation at 100*g* for 10 s. After the indicated times, cells were washed and lysed in buffer containing 1% LM (an *N*-dodecyl β-maltoside), 1% NP-40, 1 mM Na_3VO_4, 1 mM phenylmethylsulfonyl fluoride, 10 mM NaF, 10 mM EDTA, 50 mM tris-HCl (pH 7.5), and 150 mM NaCl. Detergent cell lysates were incubated overnight at 4°C with the anti-Lck monoclonal antibody 3A5 coupled to protein A–agarose (Santa Cruz Biotechnology Inc.). Samples were separated by 10% SDS–polyacrylamide gel electrophoresis (SDS-PAGE) and blotted onto nitrocellulose. For dual-color analysis, membranes were first incubated with rabbit antibody against pSrc-pY416, which corresponds to pY394 of Lck, and goat anti-rabbit IRDye 680LT, stripped for 20 min (in Restore PLUS Western Blot Stripping Buffer, Thermo Scientific) and then incubated with secondary antibody to exclude remaining anti–Src-pY416 binding. Membranes were subsequently incubated with rabbit antibody against Lck and goat anti-rabbit IRDye 800CW. Signal intensities were determined by scanning the membranes with an Odyssey infrared imager (LI-COR) and analyzing the data with the Odyssey application software. For in vitro kinase assays, freshly prepared human T lymphocytes (5×10^7 cells per sample) or Jurkat cells (2×10^7 cells per sample) were stimulated for 30 or 120 s with a 1:100 (v/v) dilution of ascites fluid of the αCD3 monoclonal antibody MEM92 (IgM, provided by V. Horejsi, Prague). In some experiments, the αCD3ε monoclonal antibody UCHT1 (10 μg/ml) was used to stimulate cells, yielding identical results. After stimulation, cells were lysed in lysis buffer supplemented with 1% NP-40 and 1% LM as detergents. Detergent lysates were subjected to immunoprecipitation with αLck antibody with 2 μg of polyclonal rabbit antibody (Upstate) used for each immunoprecipitation. After washing, the immunoprecipitates were split; 50% of the immunoprecipitates were used for Western blotting analysis, with the αLck antibody as a control, whereas the remaining 50% of the samples were resuspended in kinase buffer [20 mM tris-HCl (pH 7.5), 10 mM $MnCl_2$, 100 μM ATP, 10 μCi of $^{32}\gamma$-ATP (PerkinElmer; 3000 Ci/mmol)] and subjected to an in vitro kinase assay for 20 min at 30°C. After the kinase reaction was complete, the radiolabeled immunoprecipitates were washed four times in washing buffer [20 mM tris-HCl (pH 7.5), 20 mM EDTA, 150 mM $NaCl_2$] and subsequently subjected to SDS-PAGE and autoradiography.

Automated multidimensional fluorescence microscopy (MELK)

Jurkat cells (1×10^6/ml) were placed onto poly-L-lysine–coated cover slides and stimulated with the αCD3ε monoclonal antibody UCHT1 (5 μg/ml) or RPMI without FCS (as a negative control) at 37°C. After 5 min, the slides were transferred into ice-cold PBS to stop the stimulation. Cells were fixed with 2% paraformaldehyde (PFA; Santa Cruz Biotechnology Inc.) and permeabilized with 0.2% Triton X-100. After labeling and imaging of the first antibody set, the dye (Alexa Fluor 488) was bleached, and samples were then incubated with the next antibody. The appropriate working dilutions, incubation times, and positions within the MELK run were validated systematically with conditions suitable to MELK (*44*). Images were recorded with a toponome imaging cycler (TIC). The sample was placed on the stage of an inverted, wide-field fluorescence microscope (Leica DM IRE2, 63× oil lens with 1.40 numerical aperture). For each of the two conditions defined by application of individual droplets of cell solution, a suitable field of view was defined manually, and the corresponding XYZ positions and a transmitted light reference image were stored by the TIC Control software. A fully automated cyclic robotic process started with the incubation of the first fluorescent antibody (or tag). After a washing step, the fluorescence signals and a corresponding phase-contrast image were acquired by a cooled charge-coupled device camera (Apogee KX4, Apogee Instruments, 1× binning results in images of 2048 × 2048 pixels; final pixel size, 143 × 143 nm^2). To eliminate the specific signal of a given tag before the addition of the next, we performed a bleaching step. A post-bleaching fluorescence signal was recorded before the next incubation-imaging-bleaching cycle started with the next tag. These cycles were processed until all of the tags were applied to the sample.

The fluorescence and post-bleaching fluorescence images produced by each tag were automatically aligned pixel-wise with the corresponding phase-contrast images, reaching an alignment accuracy of 1 pixel. Fluorescence images were corrected for illumination faults with flat-field correction. Post-bleaching images were subtracted from the subsequent fluorescence tag images. Finally, cases of section artifacts were excluded as invalid by a mask-setting process. Regions of interest for T cells analyzed were defined manually, and the background-subtracted intensities for the individual tags were recorded.

Confocal imaging

Lck-deficient JCam1.6 cells expressing a biosensor were plated on poly-L-lysine–covered slides at room temperature for 5 min and immediately fixed for 10 min in PBS (pH 7.4) containing 1.5% PFA and 0.025% glutaraldehyde. Cells were permeabilized in PBS containing 0.2% Triton X-100 for 10 min, rinsed twice with PBS, and blocked with 1% bovine serum albumin in PBS (pH 7.4) for 10 min. Cells were incubated with primary antibodies including anti-Jurkat TCR monoclonal antibody C305 (IgM, provided by A. Weiss, UCSF) and antibodies against EEA1, Rab11, and Rab5 (all from BD Bioscience) for 1 hour, and cells were subsequently washed and blocked as described earlier. Specimens were then treated with a secondary antibody (DyLight 549, Dianova) for 1 hour. After washing three times with PBS, specimens were washed once in PBS (pH 8.9) and subsequently embedded. The specimens were analyzed with a confocal microscope (Leica SP2, Leica Microsystems Heidelberg). Sequential images were acquired in the corresponding wavelength channels to avoid bleed-through processes and were later merged with ImageJ software. For membrane staining, CellTracker (CM-Dil, Molecular Probes) was added to the plated cells, incubated for 5 to 10 min, washed with PBS, and fixed and scanned with a confocal microscope as described earlier.

SUPPLEMENTARY MATERIALS

www.sciencesignaling.org/cgi/content/full/6/263/ra13/DC1

Fig. S1. Two versus three lifetimes are needed to describe the fluorescence decay of an ECFP-EYFP FRET pair.

Fig. S2. Localization of the biosensor CLckY-1 at the plasma membrane.

Fig. S3. Localization of the biosensor in transfected Lck-deficient JCam1.6 cells.

Fig. S4. Conjugate formation between transfected JCam1.6 cells expressing CLckY-1 and mock-treated Raji B cells as measured with the QA detector in the FLIM setup.

Fig. S5. Lck does not coimmunoprecipitate with Csk.

REFERENCES AND NOTES

1. T. J. Molina, K. Kishihara, D. P. Siderovski, W. van Ewijk, A. Narendran, E. Timms, A. Wakeham, C. J. Paige, K. U. Hartmann, A. Veillette, D. Davidson, T. W. Mak, Profound block in thymocyte development in mice lacking p56^{lck}. *Nature* **357**, 161–164 (1992).
2. J. Lin, A. Weiss, T cell receptor signalling. *J. Cell Sci.* **114**, 243–244 (2001).
3. F. Sicheri, J. Kuriyan, Structures of Src-family tyrosine kinases. *Curr. Opin. Struct. Biol.* **7**, 777–785 (1997).
4. E. H. Palacios, A. Weiss, Function of the Src-family kinases, Lck and Fyn, in T-cell development and activation. *Oncogene* **23**, 7990–8000 (2004).
5. M. Bergman, T. Mustelin, C. Oetken, J. Partanen, N. A. Flint, K. E. Amrein, M. Autero, P. Burn, K. Alitalo, The human p50^{csk} tyrosine kinase phosphorylates p56^{lck} at Tyr-505 and down regulates its catalytic activity. *EMBO J.* **11**, 2919–2924 (1992).
6. M. Takeuchi, S. Kuramochi, N. Fusaki, S. Nada, J. Kawamura-Tsuzuku, S. Matsuda, K. Semba, K. Toyoshima, M. Okada, T. Yamamoto, Functional and physical interaction of protein-tyrosine kinases Fyn and Csk in the T-cell signaling system. *J. Biol. Chem.* **268**, 27413–27419 (1993).
7. W. Xu, S. C. Harrison, M. J. Eck, Three-dimensional structure of the tyrosine kinase c-Src. *Nature* **385**, 595–602 (1997).
8. M. J. Eck, S. K. Atwell, S. E. Shoelson, S. C. Harrison, Structure of the regulatory domains of the Src-family tyrosine kinase Lck. *Nature* **368**, 764–769 (1994).
9. H. L. Ostergaard, D. A. Shackelford, T. R. Hurley, P. Johnson, R. Hyman, B. M. Sefton, I. S. Trowbridge, Expression of CD45 alters phosphorylation of the *lck*-encoded tyrosine protein kinase in murine lymphoma T-cell lines. *Proc. Natl. Acad. Sci. U.S.A.* **86**, 8959–8963 (1989).
10. M. Shiroo, L. Goff, M. Biffen, E. Shivnan, D. Alexander, CD45 tyrosine phosphatase-activated p59^{fyn} couples the T cell antigen receptor to pathways of diacylglycerol production, protein kinase C activation and calcium influx. *EMBO J.* **11**, 4887–4897 (1992).
11. G. Hofmann, K. Schweimer, A. Kiessling, E. Hofinger, F. Bauer, S. Hoffmann, P. Rösch, I. D. Campbell, J. M. Werner, H. Sticht, Binding, domain orientation, and dynamics of the Lck SH3–SH2 domain pair and comparison with other Src-family kinases. *Biochemistry* **44**, 13043–13050 (2005).
12. A. D. Holdorf, J. M. Green, S. D. Levin, M. F. Denny, D. B. Straus, V. Link, P. S. Changelian, P. M. Allen, A. S. Shaw, Proline residues in CD28 and the Src homology (SH)3 domain of Lck are required for T cell costimulation. *J. Exp. Med.* **190**, 375–384 (1999).
13. W. Xu, A. Doshi, M. Lei, M. J. Eck, S. C. Harrison, Crystal structures of c-Src reveal features of its autoinhibitory mechanism. *Mol. Cell* **3**, 629–638 (1999).
14. J. S. Hardwick, B. M. Sefton, Activation of the Lck tyrosine protein kinase by hydrogen peroxide requires the phosphorylation of Tyr-394. *Proc. Natl. Acad. Sci. U.S.A.* **92**, 4527–4531 (1995).
15. A. Alonso, N. Bottini, S. Bruckner, S. Rahmouni, S. Williams, S. P. Schoenberger, T. Mustelin, Lck dephosphorylation at Tyr-394 and inhibition of T cell antigen receptor signaling by *Yersinia* phosphatase YopH. *J. Biol. Chem.* **279**, 4922–4928 (2004).
16. H. Xu, D. R. Littman, The kinase-dependent function of Lck in T-cell activation requires an intact site for tyrosine autophosphorylation. *Ann. N. Y. Acad. Sci.* **766**, 99–116 (1995).
17. K. Nika, C. Soldani, M. Salek, W. Paster, A. Gray, R. Etzensperger, L. Fugger, P. Polzella, V. Cerundolo, O. Dushek, T. Höfer, A. Viola, O. Acuto, Constitutively active Lck kinase in T cells drives antigen receptor signal transduction. *Immunity* **32**, 766–777 (2010).
18. Z. Ma, T. H. Finkel, T cell receptor triggering by force. *Trends Immunol.* **31**, 1–6 (2010).
19. P. A. van der Merwe, O. Dushek, Mechanisms for T cell receptor triggering. *Nat. Rev. Immunol.* **11**, 47–55 (2011).
20. W. Paster, C. Paar, P. Eckerstorfer, A. Jakober, K. Drbal, G. J. Schütz, A. Sonnleitner, H. Stockinger, Genetically encoded Förster resonance energy transfer sensors for the conformation of the Src family kinase Lck. *J. Immunol.* **182**, 2160–2167 (2009).
21. T. Zal, N. R. Gascoigne, Photobleaching-corrected FRET efficiency imaging of live cells. *Biophys. J.* **86**, 3923–3939 (2004).
22. P. I. Bastiaens, A. Squire, Fluorescence lifetime imaging microscopy: Spatial resolution of biochemical processes in the cell. *Trends Cell Biol.* **9**, 48–52 (1999).
23. F. S. Wouters, P. I. Bastiaens, Fluorescence lifetime imaging of receptor tyrosine kinase activity in cells. *Curr. Biol.* **9**, 1127–1130 (1999).
24. M. A. Goldsmith, A. Weiss, Isolation and characterization of a T-lymphocyte somatic mutant with altered signal transduction by the antigen receptor. *Proc. Natl. Acad. Sci. U.S.A.* **84**, 6879–6883 (1987).
25. A. J. Visser, S. P. Laptenok, N. V. Visser, A. van Hoek, D. J. Birch, J. C. Brochon, J. W. Borst, Time-resolved FRET fluorescence spectroscopy of visible fluorescent protein pairs. *Eur. Biophys. J.* **39**, 241–253 (2010).
26. J. W. Borst, S. P. Laptenok, A. H. Westphal, R. Kühnemuth, H. Hornen, N. V. Visser, S. Kalinin, J. Aker, A. van Hoek, C. A. Seidel, A. J. Visser, Structural changes of yellow Cameleon domains observed by quantitative FRET analysis and polarized fluorescence correlation spectroscopy. *Biophys. J.* **95**, 5399–5411 (2008).
27. S. Habuchi, M. Cotlet, J. Hofkens, G. Dirix, J. Michiels, J. Vanderleyden, V. Subramaniam, F. C. De Schryver, Resonance energy transfer in a calcium concentration-dependent cameleon protein. *Biophys. J.* **83**, 3499–3506 (2002).
28. M. Jose, D. K. Nair, C. Reissner, R. Hartig, W. Zuschratter, Photophysics of Clomeleon by FLIM: Discriminating excited state reactions along neuronal development. *Biophys. J.* **92**, 2237–2254 (2007).
29. S. P. Laptenok, J. W. Borst, K. M. Mullen, I. H. van Stokkum, A. J. Visser, H. van Amerongen, Global analysis of Förster resonance energy transfer in live cells measured by fluorescence lifetime imaging microscopy exploiting the rise time of acceptor fluorescence. *Phys. Chem. Chem. Phys.* **12**, 7593–7602 (2010).
30. M. Millington, G. J. Grindlay, K. Altenbach, R. K. Neely, W. Kolch, M. Bencina, N. D. Read, A. C. Jones, D. T. Dryden, S. W. Magennis, High-precision FLIM–FRET in fixed and living cells reveals heterogeneity in a simple CFP–YFP fusion protein. *Biophys. Chem.* **127**, 155–164 (2007).
31. D. K. Nair, M. Jose, T. Kuner, W. Zuschratter, R. Hartig, FRET-FLIM at nanometer spectral resolution from living cells. *Opt. Express* **14**, 12217–12229 (2006).
32. M. Vitali, F. Picazo, Y. Prokazov, A. Duci, E. Turbin, C. Götze, J. Llopis, R. Hartig, A. J. Visser, W. Zuschratter, Wide-field multi-parameter FLIM: Long-term minimal invasive observation of proteins in living cells. *PloS ONE* **6**, e15820 (2011).
33. O. M. Antón, L. Andrés-Delgado, N. Reglero-Real, A. Batista, M. A. Alonso, MAL protein controls protein sorting at the supramolecular activation cluster of human T lymphocytes. *J. Immunol.* **186**, 6345–6356 (2011).
34. I. A. Yudushkin, R. D. Vale, Imaging T-cell receptor activation reveals accumulation of tyrosine-phosphorylated CD3ζ in the endosomal compartment. *Proc. Natl. Acad. Sci. U.S.A.* **107**, 22128–22133 (2010).
35. S. C. Ley, M. Marsh, C. R. Bebbington, K. Proudfoot, P. Jordan, Distinct intracellular localization of Lck and Fyn protein tyrosine kinases in human T lymphocytes. *J. Cell Biol.* **125**, 639–649 (1994).

36. M. Pelosi, V. Di Bartolo, V. Mounier, D. Mège, J. M. Pascussi, E. Dufour, A. Blondel, O. Acuto, Tyrosine 319 in the interdomain B of ZAP-70 is a binding site for the Src homology 2 domain of Lck. *J. Biol. Chem.* **274**, 14229–14237 (1999).
37. D. B. Straus, A. Weiss, Genetic evidence for the involvement of the Lck tyrosine kinase in signal transduction through the T cell antigen receptor. *Cell* **70**, 585–593 (1992).
38. E. Bruyns, A. Marie-Cardine, H. Kirchgessner, K. Sagolla, A. Shevchenko, M. Mann, F. Autschbach, A. Bensussan, S. Meuer, B. Schraven, T cell receptor (TCR) interacting molecule (TRIM), a novel disulfide-linked dimer associated with the TCR–CD3–ζ complex, recruits intracellular signaling proteins to the plasma membrane. *J. Exp. Med.* **188**, 561–575 (1998).
39. K. Kemnitz, L. Pfeifer, R. Paul, F. Fink, A. Bergmann, Time- and space-correlated single-photon-counting spectroscopy. *SPIE Proc.* **2628**, 2–11 (1995).
40. K. Kemnitz, L. Pfeifer, R. Paul, M. Coppey-Moisan, Novel detectors for fluorescence lifetime imaging on the picosecond time scale. *J. Fluoresc.* **7**, 93–98 (1997).
41. J. Lakowicz, *Principles of Fluorescence Spectroscopy* (Springer, New York, ed. 3, 2006).
42. S. P. Laptenok, J. W. Borst, K. M. Mullen, I. H. M. van Stokkum, A. J. W. G. Visser, H. van Amerongen, Global analysis of Förster resonance energy transfer in live cells measured by fluorescence lifetime imaging microscopy exploiting the rise time of acceptor fluorescence. *Phys. Chem. Chem. Phys.* **12**, 7593–7602 (2010).
43. J. W. Borst, S. P. Laptenok, A. H. Westphal, R. Kühnemuth, H. Hornen, N. V. Visser, S. Kalinin, J. Aker, A. van Hoek, C. A. M. Seidel, A. J. W. G. Visser, Structural changes of Yellow Cameleon domains observed by quantitative FRET analysis and polarized fluorescence correlation spectroscopy. *Biophys. J.* **95**, 5399–5411 (2008).
44. W. Schubert, B. Bonnekoh, A. J. Pommer, L. Philipsen, R. Böckelmann, Y. Malykh, H. Gollnick, M. Friedenberger, M. Bode, A. W. Dress, Analyzing proteome topology and function by automated multidimensional fluorescence microscopy. *Nat. Biotechnol.* **24**, 1270–1278 (2006).

Acknowledgments: We thank T. Beyer for critically reading the manuscript and for the helpful discussions and J. Rudolph for performing densitometric analysis and preparing Fig. 6. **Funding:** This work was supported by collaborative research grants (SFB854, FOR521) from the German Research Society (DFG) to B.S., J.A.L., M.G., P.R., L.S., R.H., and W.Z., as well as a research grant from the State of Saxony-Anhalt (FKZ: XN0050KL/0206) to B.S. B.S. and J.A.L. are members of the SYBILLA consortium [EU 7FP] and the Magdeburg Center for Systems Biology (MaCS). Further support was provided by the Federal Ministry of Education and Research (BMBF), FKZ 13N10077, to W.Z., and the Austrian Science Fund through the EUROCORES Euromembrane program LIPIDPROD I0030 and the Erwin Schroedinger scholarship program to H.S. **Author contributions:** A.S., S.G., and R.H. performed the FLIM experiments; R.H., Y.P., and W.Z. designed and constructed the FLIM setup and analyzed the FLIM data; W.P. and H.S. provided the biosensor contructs; L.S. and M.P. performed the biochemical analysis of the Lck immunoprecipitates with the anti-Src family pY416 antibody in Fig. 5A; L.P. and P.R. analyzed the MELK data in Fig. 5, B and C; C.M. performed the functional analysis of Lck-reconstituted cells and the in vitro kinase assays in Fig. 6; and T.H., R.H., J.A.L., M.G., and B.S. designed the experiments and wrote the manuscript. **Competing interests:** The authors declare that they have no competing interests. **Data and materials availability:** Use of the plasmids encoding fluorescently tagged proteins requires a materials transfer agreement.

Submitted 13 September 2012
Accepted 31 January 2013
Final Publication 19 February 2013
10.1126/scisignal.2003607
Citation: A. Stirnweiss, R. Hartig, S. Gieseler, J. A. Lindquist, P. Reichardt, L. Philipsen, L. Simeoni, M. Poltorak, C. Merten, W. Zuschratter, Y. Prokazov, W. Paster, H. Stockinger, T. Harder, M. Gunzer, B. Schraven, T cell activation results in conformational changes in the Src family kinase Lck to induce its activation. *Sci. Signal.* **6**, ra13 (2013).

T Cell Activation Results in Conformational Changes in the Src Family Kinase Lck to Induce Its Activation

Anja Stirnweiss, Roland Hartig, Steffi Gieseler, Jonathan A. Lindquist, Peter Reichardt, Lars Philipsen, Luca Simeoni, Mateusz Poltorak, Camilla Merten, Werner Zuschratter, Yury Prokazov, Wolfgang Paster, Hannes Stockinger, Thomas Harder, Matthias Gunzer and Burkhart Schraven (February 19, 2013)

Science Signaling **6** (263), ra13. [doi: 10.1126/scisignal.2003607]